

# Genesis of tuff interval and its uranium enrichment in Upper Triassic of Ordos Basin, NW China

Shamim Akhtar<sup>1,2</sup> · Nosheen Sahir<sup>3</sup> · Xiaoyong Yang<sup>1</sup>

Received: 30 August 2016 / Revised: 20 May 2017 / Accepted: 16 June 2017 / Published online: 27 July 2017  
© Science Press, Institute of Geochemistry, CAS and Springer-Verlag GmbH Germany 2017

**Abstract** Recently measured high gamma ray values in the Yanchang Formation of the Upper Triassic in the Ordos Basin have added an interesting and controversial twist to the study of the formation's uranium enrichment and genesis. High uranium and thorium contents in the tuffaceous layer cause high gamma ray values in the Yanchang Formation. Petrographic studies, major elements, rare earth elements (REEs), and trace elements have been systematically analyzed to determine the composition, geochemical environment, and diagenetic processes of the layer. The observed color of the tuffaceous layer in the study area varies from yellow to yellowish brown. The tuff consists of matrix supported with sub-rounded to sub-angular lithic fragments. These lithic fragments probably derived from pre-existing rocks and incorporated into the tuffaceous layer during volcanic eruption. Quartz, plagioclase, and biotite were observed in well to poorly sorted form, in addition to frambooidal pyrite and organic laminae. Measured ratios of  $\text{SiO}_2/\text{Al}_2\text{O}_3$  ranged from 3.277 to 6.105 with an average of 3.738. The ratio of  $\text{TiO}_2/\text{Al}_2\text{O}_3$  varied from 0.037 to 0.201 with an average of 0.061, indicating that the sediments of the tuffaceous layer originated from an intermediate magma. REE distribution patterns show sharp

negative Eu anomalies, indicating a reducing environment, which is suitable for uranium deposition. A reducing environment was confirmed by black shale in the base of the Yanchang Formation. Such black shale has high organic matter content that can take kerogen from mudstone and provide a reducing environment for uranium enrichment in the tuffaceous layer. Moreover, negative Eu anomalies and the REE patterns indicate a subduction-related volcanic arc environment as the magma source of the tuffaceous layers. High values of Rb, Ba, and Sr might be the result of fluid phase activities; low values of Hf and Eu indicate the involvement of crustal material during diagenesis of the tuff. Discrimination diagrams ( $\text{Th/Yb}$  vs  $\text{Ta/Yb}$ ,  $\text{Th/Hf}$  vs  $\text{Ta/Hf}$ ) suggest an active continental margin as the tectonic setting of source volcanoes. Plots of Nb versus Y, Rb versus  $\text{Y} + \text{Nb}$ ,  $\text{TiO}_2$  versus Zr, and  $\text{Th/Yb}$  versus  $\text{Nb/Yb}$  of the tuffaceous content point to calc-alkaline continental arc-related magmatism. We concluded that uranium enrichment in the tuffaceous layer was supported by oxidation-reduction.

**Keywords** Tuffaceous layer · Gamma ray values · Uranium enrichment · Yanchang Formation · Ordos Basin

✉ Xiaoyong Yang  
xyyang@ustc.edu.cn

<sup>1</sup> CAS Key Laboratory of Crust-Mantle Materials and Environments, University of Science and Technology of China, Hefei 230026, China

<sup>2</sup> Institute of Geology, University of the Azad Jammu & Kashmir, City Campus, Muzaffarabad 13100, Pakistan

<sup>3</sup> School of Engineering and Technology, Asian Institute of Technology, Bangkok Metropolitan Area, Khlong Luang, Thailand

## 1 Introduction

In the Ordos Basin, Permian, Triassic, Jurassic, and Cretaceous rocks show high gamma ray anomalies, indicating the presence of uranium (Zhao 2005; Zhao et al. 2006). Associated large-scale uranium deposits are found in the Zhilou Formation of Jurassic time in the Dongsheng and Huangling areas of the Ordos Basin. The recent discovery in the Yanchang Formation of a high-potential hydrocarbon reservoir that also has high gamma ray values, became

an interesting and controversial topic among geologists. The Yanchang Formation is divided into ten members—Chang 10 to Chang 1 from top to bottom. High gamma ray values were found in Chang 8, Chang 7, Chang 6, and Chang 4 + 5 in different regions of the Ordos Basin. There is no universally accepted definition of a high gamma ray reservoir so authors have presented different arguments for this Triassic age reservoir. High gamma ray sandstone of the Yanchang Formation might be the result of re-deposition of sedimentary tuff (Zhang et al. 2010). Gamma ray content in sedimentary rocks can be measured through pelite. Rocks with normal gamma ray content show pelite values up to 30%; if the pelite content values exceed 40%, then it is deemed high gamma ray sandstone (Zhang et al. 2010). The mud and clay content distinguish high gamma ray sandstone. High gamma ray values might also result from high content of feldspar, uranium, and thorium of the tuffaceous layer in the Yanchang Formation (Li et al. 2006; Qiu et al. 2009; Sun et al. 2010; Zhang et al. 2010). Very few tuffaceous samples of well Y91 show high gamma ray values so the high gamma ray values of the Yanchang Formation are proposed to be the result of high content of heavy elements like uranium and thorium in zircon, rather than feldspar and clay minerals (Liu et al. 2013). However, this theory is inconsistent with gamma ray spectrum logging of the highly radioactive Yanchang sandstone (Li et al. 2006; Qiu et al. 2009; Sun et al. 2010). According to this second set of results, high gamma ray values are related to high uranium and thorium content in the sandstone and show no genetic relationship with zircon. The high gamma ray values of the tuffaceous layers at the bottom of Chang 7 have been previously confirmed (Qiu et al. 2014).

## 2 Regional geology of the Ordos Basin

The Ordos Basin is the western block of the north China Craton and is known as the intracratonic basin (Li et al. 1995). It lies in the transitional zone between an extensional rift basin and a compressional basin. The Ordos Basin is affected by the tectonic activity of eastern and western China (Li et al. 1995; Yang 2002; Yuan et al. 2007). N-S striking folds, faults, depressions, and uplifts separate eastern and western China, as established by the study of stratigraphy and geophysical and structural characteristics (Li and Li 2008). The Ordos Foreland Basin formed as a result of collision of the Tethys tectonic field of southwest China with the north China and Yangtze Blocks (Li et al. 1995; Liu 1998). It is a stable rigid block with no major faulting and prominent deformation on the margins (Li et al. 1995). The Basin is surrounded by active

tectonic belts. It is bound to the north by the Inner Mongolia-Dixing'anling fold system, to the south by the Qilian–Qinling fold system, to the east by the Shanxi block, and to the west by the Alashan block (Cai et al. 2007; Yang et al. 2009; Li and Li 2011) (Fig. 1A). Similar to the Ordos Basin, strata of the Dongsheng uranium deposit dip slightly (Fig. 1B).

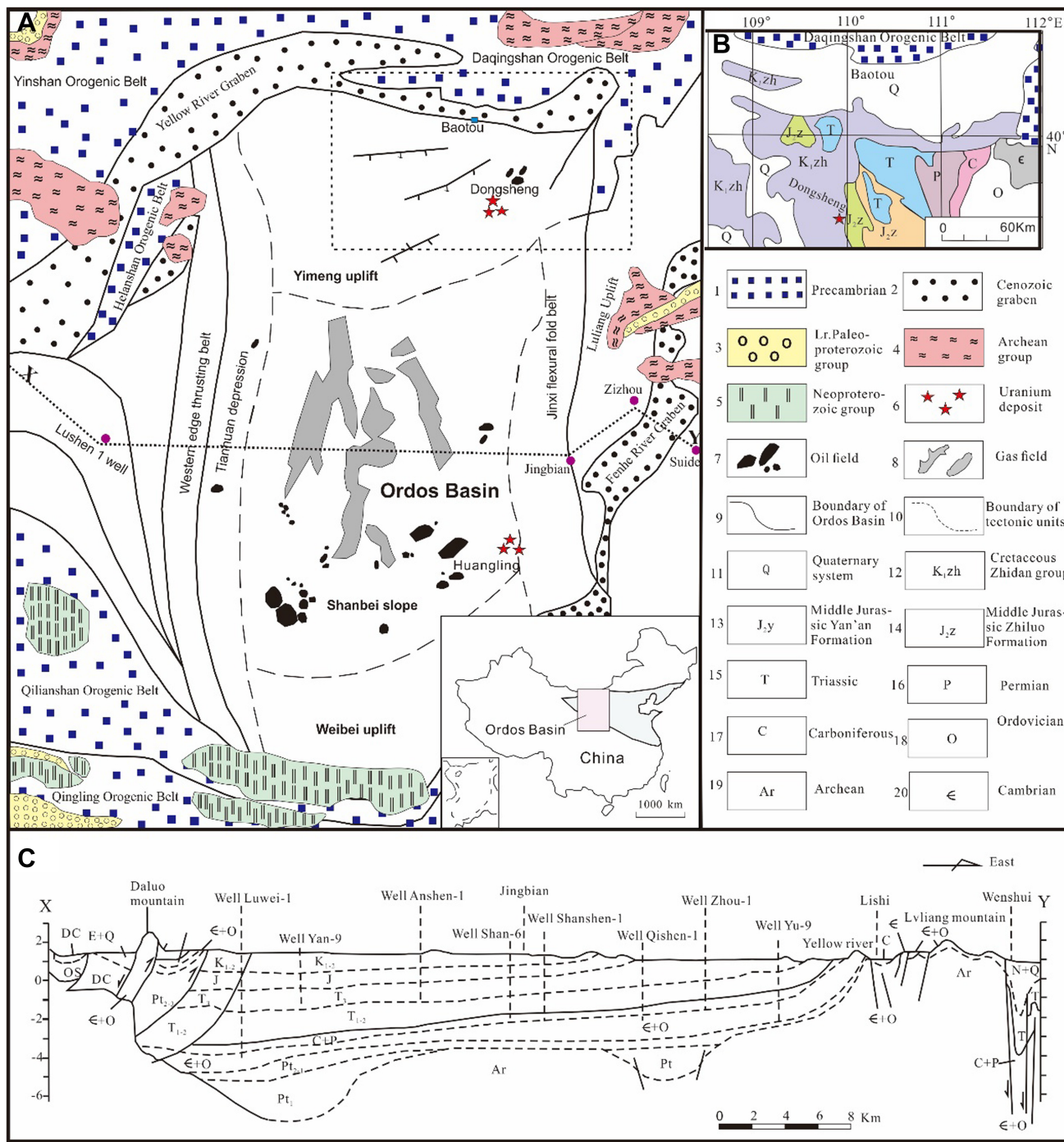
The basement rocks of the Ordos Basin are metamorphic crystalline rocks of the Neoarchean, Paleoproterozoic, Meso-Neoproterozoic series with average thickness of 4 to 5 km (Yang 2002; Wang et al. 2015). In the cross-sectional profile of the Ordos Basin, aeromagnetic anomalies indicate that the basement rocks show three uplifts—the Yulin–Daotu, Dongsheng, and Yijinhuoluo—and two depression—the Yanchuan–Yulin and Baotou—from north to south (Wang et al. 2015) (Fig. 1C).

One side of the Ordos Basin is steep with a turbidite sequence while the other side is a gentle slope. The gentle slope is basically fluvial facies sandstone, favorable for uranium mineralization. The sediments of the Ordos Basin were deposited on a crystalline basement beginning in the Archean to Early Proterozoic and ending in the Mid-Cenozoic. The thickness of the sediments deposited in Middle–Upper Proterozoic and Mid-Cenozoic is up to 6000 m (Yang et al. 2009). A detailed stratigraphy of the Ordos Basin is presented in Fig. 2.

The Yanchang Formation is composed of sandstone, siltstone, mudstone, and the tuff layer with an estimated thickness of about 1000 to 1300 m (Qiu et al. 2014). PetroChina Changqing Oilfield Company subdivided the Yanchang Formation into 10 members (Chang 10 to Chang 1) on the basis of reservoir characteristics (Li et al. 2009; Zou et al. 2012; Qiu et al. 2014). Chang 7 is the lacustrine black shale deposit containing the high gamma ray tuffaceous interval (Zhang et al. 2006).

## 3 Petrology of high gamma ray sandstone of the Yanchang Formation

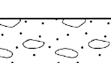
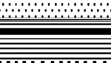
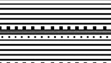
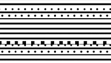
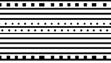
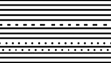
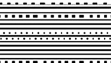
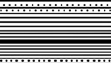
The Upper Triassic Yanchang Formation is comprised of sandstone, mudstone, blackshales, and a tuffaceous layer. Individual beds of the tuffaceous layer vary from 0.2 to 45 cm. The observed color of the tuffaceous layer in the study area is from yellow to yellowish brown. Thin section study of the tuff revealed a matrix supported with sub-rounded to sub-angular lithic fragments (Fig. 3). These lithic fragments probably derived from pre-existing rocks and incorporated into the tuffaceous layer during volcanic eruption. Quartz, plagioclase, and biotite were present in well to poorly sorted form. In addition to these minerals, framboidal pyrite and organic laminae were observed.



**Fig. 1** **A** Geologic map of the Ordos Basin (modified after Cai et al. 2007; Yang et al. 2009; Li and Li 2011). **B** Geologic map of the Dongsheng area (modified after Li and Li 2011). **C** East–west cross-section of the Ordos Basin, mapped by seismic tomography and drilling wells (modified after Wang et al. 2015)

Plagioclase content of the high gamma ray sandstone is up to 50% (Zhang et al. 2010). A few zircon inclusions were observed within quartz grains (Fig. 3E). Through diagenetic evolution, the tuffaceous layer might have been altered to clay minerals such as illite, smectite, and a

mixture of illite and smectite. A sandstone thin section showed mineral alteration such as sericitization, with sericite replacing K-feldspar (Fig. 3A, B). Mineral alteration and zircon inclusions indicate the high uranium content of the tuffaceous layer.

Stratigraphic sequence					Rock description
Group	System	Series	Formation	Column	
Cenozoic	Quaternary		(0–280m)		Loess, muddy clay, brown sand and conglomerate at the bottom
	Tertiary		(150–360m)		Reddish brown mudstone, sandy clay and conglomerate at the bottom occasionally
Mesozoic	Cretaceous	Lower	Zhidan (0–1280m)		Brownish red, mid-coarse grained sandstone and brownish red and bluish gray argillaceous rocks, locally interbedded with conglomeratic sandstone
	Jurassic	Middle	Anding (80–150m)		Mainly brownish red mudstone, intercalated with silty and fine-grained sandstone in the lower part, and various colored marl in the upper part
			Zhiluo (200–400m)		Grayish green, fine-grained sandstone, argillaceous sandstone intercalated with grayish green mudstone and arenaceous mudstone in the upper part, gray mudstone, arenaceous mudstone intercalated with gray fine-grained sandstone and argillaceous sandstone in the lower part
		Lower	Yanan (250–300m)		Dark gray mudstone and carbonaceous mudstone intercalated with coal seams, interbedded with grayish, grayish white fine-middle grained sandstone and arenaceous sandstone, very thick sandstone at the bottom
	Triassic	Upper	Yanchan (800–1400m)		Dark gray mudstone and carbonaceous mudstone intercalated with coal seam, Interbedded with gray fine-grained sandstone and argillaceous sandstone in different thickness locally with coal seam
		Middle	Zhifang (210–300m)		Gray, dark gray and brown mudstone and arenaceous mudstone intercalated with gray and pink fine-middle grained sandstone and arenaceous sandstone with different thickness
		Lower	Heshanggou (100–130m)		Purple red sandy mudstone and sandstone, with grain size coarsening downwards, with fine-grained conglomerate locally
			Liujiagou (230–300m)		Interbeds of brown argillaceous sandstone and siltstone
Paleozoic	Permian	Upper	Shiqianfang (260–290m)		Brownish red mudstone intercalated with light pink fine-grained sandstone in the upper part, brownish red mudstone intercalated with light gray fine-grained sandstone
		Middle	Upper Shihezi (130–140m)		Thick brown and dark brown mudstone intercalated with light gray fine grained sandstone
			Lower Shihezi (140–150m)		Light gray fine-grained sandstone, grayish white middle-grained sandstone, conglomeratic coarse-grained sandstone intercalated with light gray and various colored mudstone
		Lower	Shanxi (80–110m)		Thick dark gray mudstone, grayish black mudstone intercalated with grayish white middle- fine-grained sandstone and thin coal seam
			Taiyuan (25–40m)		Dark-gray limestone intercalated with black mudstone at the top grayish black mudstone, coal seam intercalated with gray fine-grained sandstone
	Carboniferous	Upper	Benxi (10–25m)		Coal seam and grayish black carbonaceous mudstone at the top, aluminiferous mudstone at the bottom
	Odovician		(500–600m)		Dark gray limestone, gray argillaceous dolomite, muddy dolomite, light gray dolomite, intercalated with evaporite in the lower part

**Fig. 2** Detailed stratigraphy of the Ordos Basin. After Yang et al. (2009)

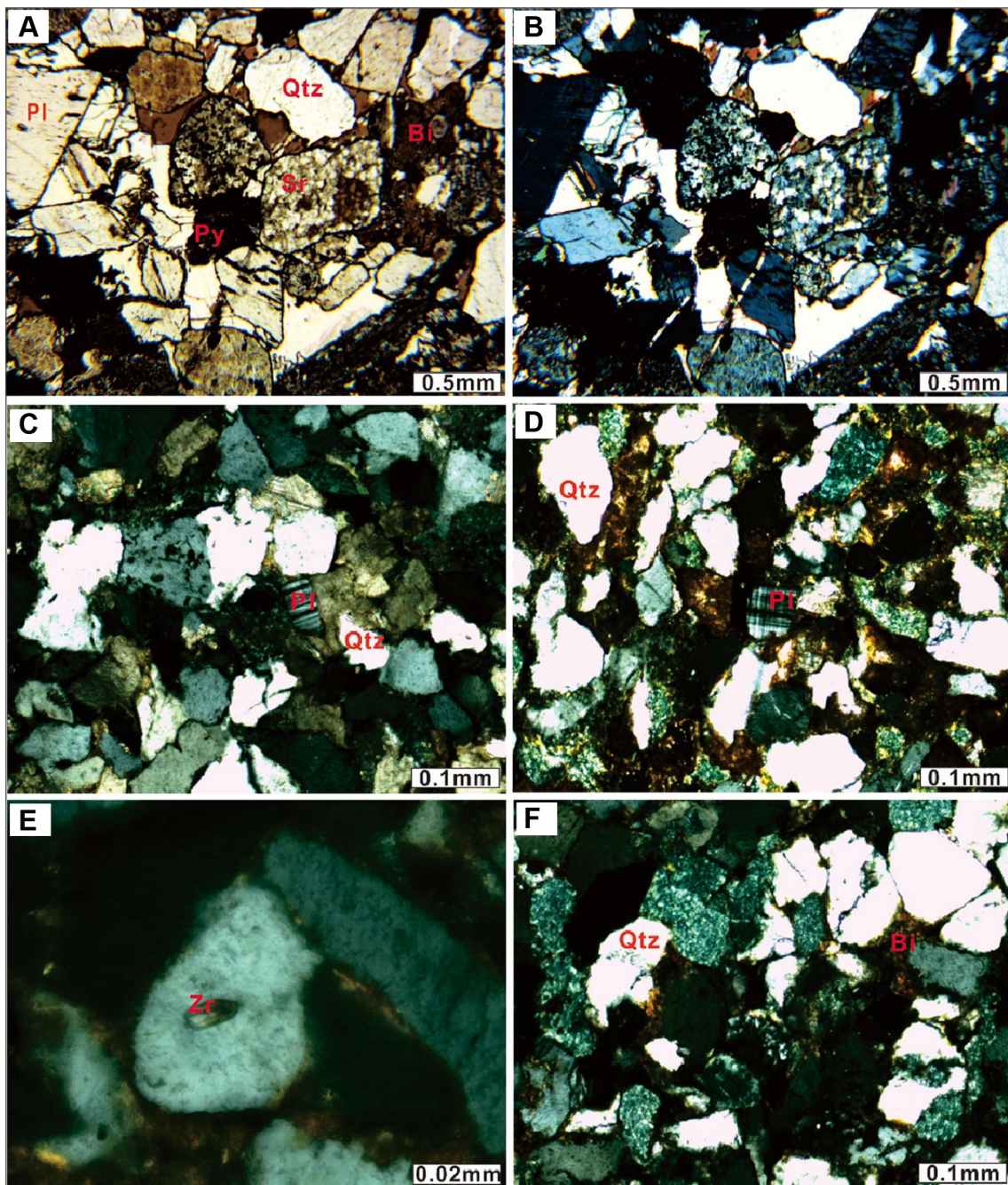


**Fig. 3** Thin sections showing primary minerals and altered minerals of the tuffaceous sandstone of the Yanchang Formation. *Qtz* quartz, *Pl* plagioclase, *Bt* biotite, *Sr* sericite, *Py* pyrite. **A** and **B** are images of YCF-05, a medium-grained feldspathic sandstone; sericitization and plagioclase twins are common. **C** and **D** are images of YCF-03 and YCF-04, respectively, showing sub-rounded to sub-angular quartz grains and plagioclase twinnings. **E** and **F** are YCF-07-1 and YCF 07-3 respectively, showing zircon inclusion in quartz grains and biotite

#### 4 Geochemistry of the tuffaceous layer of the Yanchang Formation

##### 4.1 Sampling and methodology

To study the genesis of the tuffaceous layer, we collected 14 well samples from the study area. Petrographic

descriptions of the well samples are in Table 1. Samples were analyzed for major elements, trace elements, and rare earth elements (REEs) in ALS Geochemistry Laboratory of Guangzhou. Major elements were determined by X-ray fluorescence (XRF). Samples were crushed in steel jaw crushers to <200 mesh. Mixtures of whole rock powder (0.5 g) and  $\text{LiB}_4\text{O}_7 + \text{LiBO}_2$  were prepared in a glass disk

**Table 1** Petrographic description of samples of the tuffaceous layer (Chang 7) of the Triassic Yanchang Formation, Dongsheng area, Ordos Basin

Sample	Petrographic description
YCF-01	Mudstone
YCF-02	Mudstone
YCF-03	Tuffaceous sandstone
YCF-04	Tuffaceous sandstone
YCF-05	Sandstone
YCF-06	Mudstone
YCF-07-1	Tuffaceous sandstone
YCF-07-2	Tuffaceous sandstone
YCF-07-3	Mudstone
YCF-08-1	Tuffaceous sandstone
YCF-08-2	Tuffaceous sandstone
YCF-08-3	Mudstone
YCF-09	Tuffaceous sandstone
YCF-10	Sandstone

for XRF analysis with an AXIOS Minerals spectrometer. Analytical uncertainties during this process were generally within 0.1% to 1% (RSD).

For the analysis of trace elements, whole rock samples were dissolved in distilled HF + HNO<sub>3</sub> in Teflon screwcap capsules at 200 °C for several days, dried, and then digested with HNO<sub>3</sub> at 150 °C for one day. The final solution was obtained after this procedure and diluted to 80 g with a mixture of 1 ml internal standard solution of the single element Rh, with a dilution factor of 1/250 in 2% ultrapure HNO<sub>3</sub>. The diluted solution was then analyzed by inductively coupled plasma-mass spectrometry (ICP-MS) (Element, Finnigan MAT). Uncertainties in this analysis were less than ±5%.

#### 4.2 Origin of the tuffaceous layer

Tuffaceous layer samples returned SiO<sub>2</sub> contents of 28.27% to 61.04% (Table 2), reflecting different quartz contents in the samples. The variation of quartz in the tuffaceous layer indicates its different sources. The tuffaceous layer samples also contained mudstone and high oxygen content indicating the presence of clay minerals. The most common clay minerals were illite and smectite. The presence of shale is the result of the diagenetic product smectite (Qiu et al. 2014). Samples were high in aluminum and alkali (Table 2). The ratio of SiO<sub>2</sub>/Al<sub>2</sub>O<sub>3</sub> ranged from 3.277 to 6.105 with an average of 3.738; TiO<sub>2</sub>/Al<sub>2</sub>O<sub>3</sub> varied from 0.037 to 0.201 with average of 0.061, indicating tuffaceous layer

**Table 2** Major elements of tuffaceous layer samples

Sample	SiO <sub>2</sub> (%)	TiO <sub>2</sub> (%)	Al <sub>2</sub> O <sub>3</sub> (%)	Fe <sub>2</sub> O <sub>3</sub> (%)	CaO (%)	MgO (%)	Na <sub>2</sub> O (%)	K <sub>2</sub> O (%)	P <sub>2</sub> O <sub>5</sub> (%)	MnO (%)	Σ (%)	SiO <sub>2</sub> /Al <sub>2</sub> O <sub>3</sub>	TiO <sub>2</sub> /Al <sub>2</sub> O <sub>3</sub>
YCF-01	61.04	0.78	18.28	5.23	1.40	2.5	3.93	4.99	0.24	0.07	98.46	3.34	0.04
YCF-02	58.35	0.83	16.64	7.57	1.47	2.97	4.45	3.00	0.26	0.11	95.65	3.51	0.05
YCF-03	52.86	0.96	16.01	7.80	1.18	3.31	5.76	3.37	0.20	0.09	91.54	3.30	0.06
YCF-04	55.82	0.84	17.03	8.11	1.49	3.7	3.04	3.07	0.25	0.1	93.45	3.28	0.05
YCF-05	59.54	0.85	17.94	7.01	1.5	2.61	3.60	3.93	0.27	0.08	97.33	3.32	0.05
YCF-06	60.72	0.74	18.17	6.90	1.08	2.95	3.87	4.82	0.18	0.08	99.51	3.34	0.04
YCF-07-1	56.85	0.76	16.06	7.11	0.93	3.15	2.14	3.73	0.26	0.1	91.09	3.54	0.05
YCF-07-2	56.63	0.71	16.05	7.00	0.90	3.23	2.02	3.72	0.18	0.07	90.51	3.53	0.04
YCF-07-3	56.25	0.98	15.02	5.67	0.77	3.74	2.49	3.93	0.25	0.08	89.18	3.75	0.07
YCF-08-1	57.85	0.76	16.23	7.44	1.01	3.43	1.99	3.97	0.19	0.1	92.97	3.56	0.05
YCF-08-2	57.84	0.80	16.62	7.35	1.03	3.47	1.85	3.55	0.23	0.07	92.81	3.48	0.05
YCF-08-3	57.09	0.60	16.13	7.01	0.95	3.36	1.96	3.29	0.24	0.1	90.73	3.54	0.04
YCF-09	52.52	0.79	11.05	1.96	14.47	0.63	3.26	2.61	0.06	0.07	87.42	4.75	0.07
YCF-10	28.27	0.93	4.63	5.48	27.52	18.85	5.29	1.16	0.17	0.06	92.36	6.11	0.20

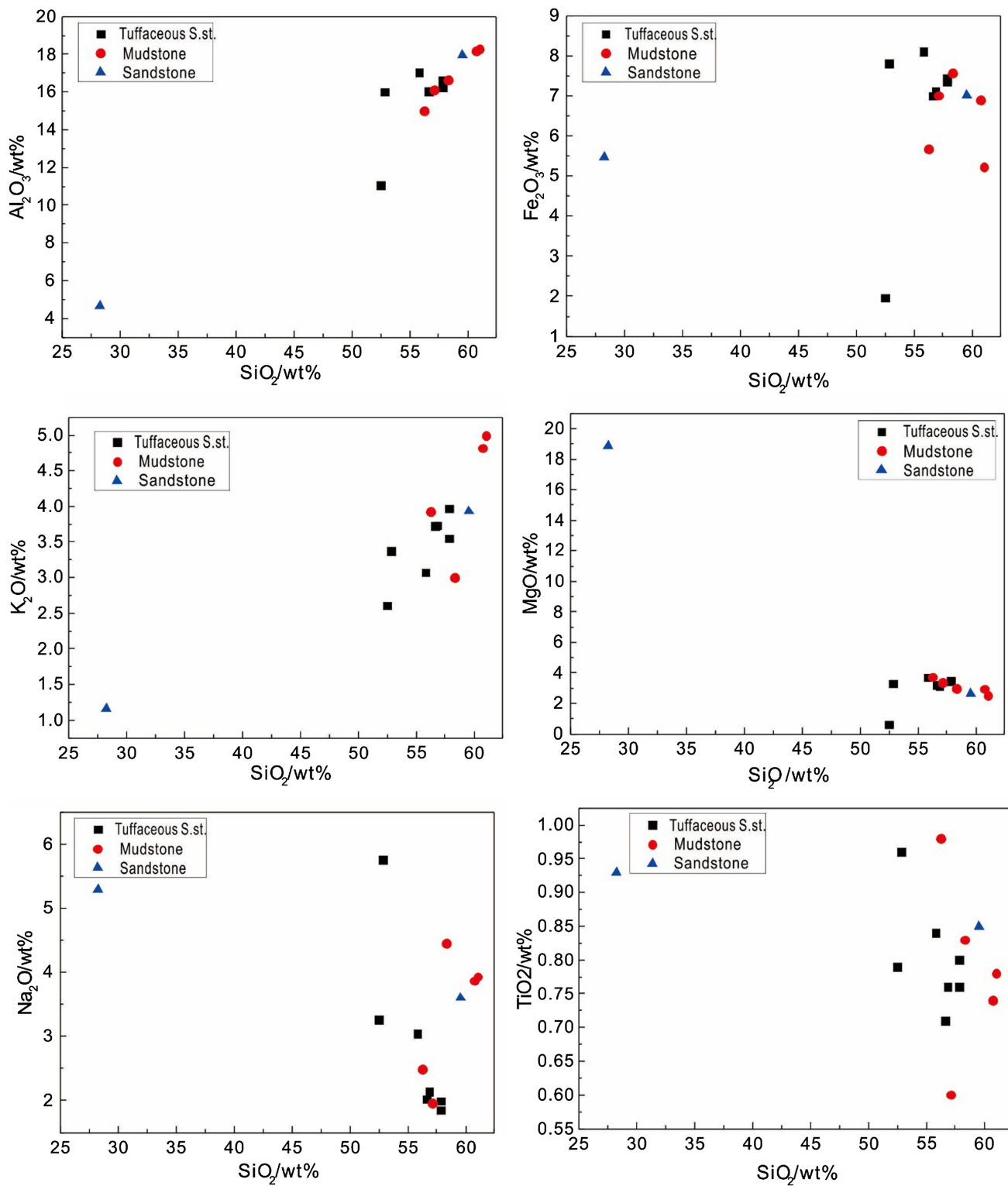


**Fig. 4** Correlation of major elements of the tuffaceous layer with its  $\text{SiO}_2$  content

sediments originated from an *intermediate* magma (Fig. 4). A correlation was found between major elements of the tuffaceous layer and silica content. Al and

K showed a positive correlation with  $\text{SiO}_2$ ; Fe, Mg, Ti, and Na showed weak negative or no correlation with  $\text{SiO}_2$ .

#### 4.3 Depositional environment and the cause of uranium enrichment in the tuffaceous layer

REE data contribute to understanding the geochemical environment of the tuffaceous layer. Compositional values of REEs are listed in Table 3. Numerical values were also calculated for  $\Sigma$ REE,  $\Sigma$ La–Nd,  $\Sigma$ Sm–Ho,  $\Sigma$ Er–Lu, LREE/HREE,  $\delta$ Ce, and  $\delta$ Eu after Wang et al. (1989). Ce and Eu anomalies were calculated after Taylor and McLennan (1985), formula:  $\delta$ Ce =  $C_{\text{Ce}}/(La_N \times Nd_N)^{1/2}$  and  $\delta$ Eu =  $Eu_N/(Sm_N \times Gd_N)^{1/2}$ .  $\Sigma$ REE values ranged from 58.02 to 215.43.  $\Sigma$ La–Nd values ranged from 51.32 to 186.05.  $\Sigma$ Sm–Ho values ranged from 5.21 to 25.52 and  $\Sigma$ Er–Lu from 1.49 to 6.65. Variations of these values indicate that uranium-enriched samples have high concentrations of LREEs as compared to HREEs; calculated

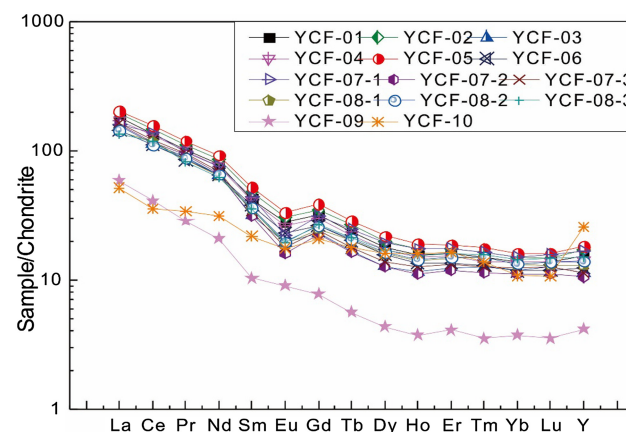


**Fig. 5** Rare earth elements of the tuffaceous layer of the Upper Triassic Yanchang Formation

**Table 3** Rare earth element data for tuffaceous layer samples

Sample	La	Ce	Pr	Nd	Sm	Eu	Gd	Tb	Dy	Ho	Er	Tm	Yb	Lu
YCF-01	43.1	81.7	9.66	36.4	6.51	1.63	6.49	0.88	4.50	0.88	2.62	0.38	2.35	0.35
YCF-02	46.3	89.6	10.45	39.7	7.29	1.77	7.12	0.99	5.02	0.99	2.88	0.42	2.53	0.37
YCF-03	37.4	69.3	8.41	30.3	4.83	1.12	4.73	0.63	3.23	0.65	2.06	0.32	2.02	0.32
YCF-04	40.8	80.5	9.44	35.1	6.25	1.51	6.09	0.83	4.29	0.84	2.51	0.35	2.31	0.35
YCF-05	48.2	95.7	11.3	43.1	7.99	1.93	7.91	1.07	5.55	1.07	3.07	0.45	2.72	0.41
YCF-06	34.0	68.2	8.06	30.5	5.82	1.33	5.40	0.75	3.95	0.76	2.22	0.33	1.99	0.30
YCF-07-1	37.6	83.3	9.33	35.3	6.68	1.28	6.39	0.92	4.89	0.98	2.90	0.42	2.57	0.40
YCF-07-2	38.3	70.8	8.89	30.9	4.79	0.93	4.6	0.61	3.19	0.63	1.97	0.29	1.88	0.28
YCF-07-3	38.8	74.5	9.04	32.3	5.19	1.04	4.94	0.67	3.50	0.71	2.17	0.32	2.08	0.32
YCF-08-1	33.5	72.0	8.17	29.8	5.38	1.09	5.07	0.75	4.03	0.80	2.43	0.38	2.24	0.33
YCF-08-2	34.0	67.3	8.26	30.5	5.54	1.14	5.34	0.77	4.13	0.81	2.48	0.38	2.25	0.35
YCF-08-3	31.6	71.7	7.72	29.0	5.43	1.12	5.47	0.79	4.37	0.87	2.67	0.4	2.45	0.37
YCF-09	13.9	25.0	2.72	9.7	1.58	0.52	1.59	0.21	1.10	0.21	0.68	0.09	0.63	0.09
YCF-10	12.2	21.6	3.20	14.5	3.34	1.02	4.22	0.66	4.10	0.90	2.72	0.35	1.83	0.27
Sample	Y	$\Sigma$ REE	$\Sigma$ La–Nd	$\Sigma$ Sm–Ho	$\Sigma$ Er–Lu	LREE/HREE	$\delta$ Ce	$\delta$ Eu						
YCF-01	24.0	197.45	170.86	20.89	5.70	9.70	2.06	0.25						
YCF-02	26.6	215.43	186.05	23.18	6.20	9.60	2.09	0.25						
YCF-03	17.8	165.32	145.41	15.19	4.72	10.84	2.06	0.23						
YCF-04	22.2	191.17	165.84	19.81	5.52	9.88	2.13	0.24						
YCF-05	28.5	230.47	198.3	25.52	6.65	9.36	2.10	0.24						
YCF-06	19.4	163.61	140.76	18.01	4.84	9.42	2.12	0.24						
YCF-07-1	26.2	192.96	165.53	21.14	6.29	8.91	2.29	0.20						
YCF-07-2	16.5	168.06	148.89	14.75	4.42	11.50	2.06	0.20						
YCF-07-3	17.7	175.58	154.64	16.05	4.89	10.94	2.10	0.21						
YCF-08-1	20.4	165.97	143.47	17.12	5.38	9.35	2.28	0.21						
YCF-08-2	21.7	163.25	140.06	17.73	5.46	8.89	2.09	0.21						
YCF-08-3	23.5	163.96	140.02	18.05	5.89	8.43	2.37	0.21						
YCF-09	6.5	58.02	51.32	5.21	1.49	11.61	2.15	0.33						
YCF-10	40.0	70.91	51.5	14.24	5.17	3.71	1.62	0.27						

**Table 4** Trace element data for tuffaceous layer samples

Sample	YCF-01	YCF-02	YCF-03	YCF-04	YCF-05	YCF-06	YCF-07-1	YCF-07-2	YCF-07-3	YCF-08-1	YCF-08-2	YCF-08-3	YCF-09	YCF-10
Rb	114	114	205	136	117	95.6	227	222	257	188	207	238	79.9	6.7
Pb	24	24	28	22	25	22	27	28	29	28	29	31	16	4
Th	11.1	11.65	12.9	11.45	11.75	9.15	15.95	13.1	14.45	13.7	14.95	16.1	3.18	1.1
U	2.38	2.18	2.22	2.19	2.36	2.08	4.44	4.25	3.73	4.22	3.74	4.1	0.85	20.9
Hf	5.0	4.9	3.6	4.7	5.2	4.8	5.0	3.3	4.0	5.2	4.8	4.8	1.4	0.9
La	43.1	46.3	37.4	40.8	48.2	34	37.6	38.3	38.8	33.5	34	31.6	13.9	12.2
Ba	997	964	1060	2210	1010	935	733	8.11	893	734	722	724	849	148
Ce	81.7	89.6	69.3	80.5	95.7	68.2	83.3	70.80	74.5	72	67.3	71.7	25.0	21.6
Pr	9.66	10.45	8.41	9.44	11.3	8.06	9.33	8.89	9.04	8.17	8.26	7.72	2.72	3.2
Nd	36.4	39.7	30.3	35.1	43.1	30.5	35.3	30.9	32.3	29.8	30.5	29.0	9.7	14.5
Eu	1.63	1.77	1.12	1.51	1.93	1.33	1.28	0.93	1.04	1.09	1.14	1.12	0.52	1.02
Nb	12.9	13.3	12.6	13.5	13.4	11.5	14.4	11.6	12.9	13.1	13.8	14.3	3.5	6.9
Sr	339	324	280	357	334	322	194	214	214	228	223	205	491	252
Zr	178	175	122	163	187	171	171	111	136	183	164	163	52	41
Ta	1.0	1.0	1.0	1.0	1.0	0.9	1.2	0.9	1.1	1.1	1.1	1.2	0.3	0.5
Sm	6.51	7.29	4.83	6.25	7.99	5.82	6.68	4.79	5.19	5.38	5.54	5.43	1.58	3.34
Gd	6.49	7.12	4.73	6.09	7.91	5.4	6.39	4.6	4.94	5.07	5.34	5.47	1.59	4.22
Er	2.62	2.88	2.06	2.51	3.07	2.22	2.9	1.97	2.17	2.43	2.48	2.67	0.68	2.72
Y	24.0	26.6	17.8	22.2	28.5	19.4	26.2	16.5	17.7	20.4	21.7	23.5	6.5	40.0
Sample	YCF-01	YCF-02	YCF-03	YCF-04	YCF-05	YCF-06	YCF-07-1	YCF-07-2	YCF-07-3	YCF-08-1	YCF-08-2	YCF-08-3	YCF-09	YCF-10
Cr	80	80	80	80	80	70	70	70	60	70	70	70	20	20
Co	14.7	16.7	18.1	17.6	16.9	15.1	16.5	14.9	17.1	17	14.1	21.2	4.5	4.3
Ni	32	35	38	37	36	33	32	39	36	30	31	33	8	36
Zn	96	96	106	104	109	75	111	114	113	112	106	114	59	192
Yb	2.35	2.53	2.02	2.31	2.72	1.99	2.57	1.88	2.08	2.24	2.25	2.45	0.63	1.83
Y + Nb	36.9	39.9	30.4	35.7	41.9	30.9	40.6	28.1	30.6	33.5	35.5	37.8	10	46.9
Nb/Yb	5.49	5.26	6.24	5.84	4.93	5.78	5.60	6.17	6.20	5.85	6.13	5.84	5.56	3.77
Th/Yb	4.72	4.60	6.39	4.96	4.32	4.60	6.21	6.97	6.95	6.12	6.64	6.57	5.05	0.60
Ta/Hf	0.20	0.28	0.21	0.19	0.19	0.24	0.27	0.28	0.21	0.23	0.25	0.21	0.56	
Th/Hf	2.22	2.38	3.58	2.44	2.26	1.91	3.19	3.97	3.61	2.63	3.11	3.35	2.27	1.22
Ta/Yb	0.43	0.40	0.50	0.43	0.37	0.45	0.47	0.48	0.53	0.49	0.49	0.49	0.48	0.27
Th/Yb	4.72	4.60	6.39	4.96	4.32	4.60	6.21	6.97	6.95	6.12	6.64	6.57	5.05	0.60
Nb/Y	0.54	0.50	0.71	0.61	0.47	0.59	0.55	0.70	0.73	0.64	0.64	0.61	0.54	0.17
TiO <sub>2</sub>	0.78	0.83	0.96	0.84	0.85	0.74	0.76	0.71	0.98	0.76	0.80	0.60	0.79	0.93
Zr/TiO <sub>2</sub>	228.21	210.84	127.08	194.05	220.00	231.08	225.00	156.34	138.78	240.79	205.00	271.67	65.82	44.09

values show the following trend:  $\Sigma\text{La-Nd} > \Sigma\text{Sm-Ho} > \Sigma\text{Er-Lu}$ . As REEs mostly share geochemical properties, Ce and Eu anomalies were calculated to indicate oxidizing and reducing environments, respectively. Values of  $\delta\text{Ce}$  fluctuated between 1.62 and 2.36 and  $\delta\text{Eu}$  between 0.195 and 0.328 (Table 3). REEs of selected samples measured by high precision ICP-MS were normalized by chondrite values (Sun and McDonough 1989) and plotted in Fig. 5.

The REE distribution of most tuffaceous sandstone, sandstone, and mudstone samples display a similar trend including sharp negative Eu anomalies. Eu acts as a boundary between LREEs and HREEs, with LREEs to the left forming a steep slope, while normalized HREE values have a flatter trend. Two samples, YCF-09 (tuff) and YCF-10 (sandstone), show a different trend. Negative Eu anomalies indicate a reducing environment suitable for uranium deposition. Moreover, the negative Eu anomalies and REE distribution suggest a subduction-related volcanic arc environment for the source magma of tuffaceous material (Qiu et al. 2014).

The tuffaceous layer is bookended by sandstone at the bottom and black shale at the top. Volcanic ash might have been transported by wind and deposited in sub-aqueous conditions. According to Swanson (1956) and Disnar and Sureau (1989), the black shale has a high uranium content. Black shale is closely associated with organic matter that provides a reducing environment for uranium enrichment (Coveney and Martin 1983; Coveney et al. 1987; Coveney and Glascock 1989; Doveton and Merriam 2004). Black shales of the Yangtze Block of Lower Silurian and Lower Cambrian have uranium content of  $>10 \mu\text{g/g}$  (Liu 1992). Organic matter content was further confirmed by microscopically observed pyrite (Fig. 3A). According to Hu (2010), the total organic content (TOC) of Chang 7 is as high as 40%. Organic matter acts as a powerful reductant and has a close relationship with various mineral deposits, particularly sandstone-hosted uranium deposits (Leventhal 1993; Spirakis 1996). Almost all types of solid bitumen, some coal and humic acid are important for reduction and mineralization of uranium (Li et al. 2009). Organic matter controls the oxidation-reduction state (Eh) of mineralization (Spirakis 1996). In the case of the Yanchang Formation, organic matter takes kerogen from mudstone and provides a reducing environment for uranium enrichment in the tuffaceous layer.

#### 4.4 Trace elements

Tuffaceous layer samples had high contents of Rb, Pb, Zr, Ba, Zn, and Sr, indicating fluid phase activities (Lai et al. 2010), and low contents of Hf, Eu, and Ta, indicating the involvement of crustal material during diagenetic processes

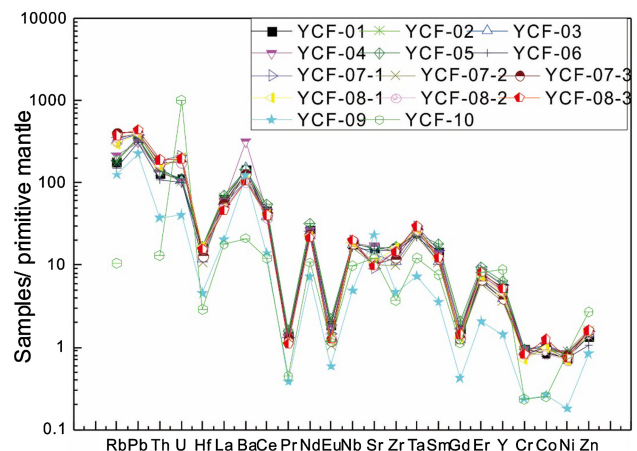


**Fig. 6** Spider diagram for trace elements of the tuffaceous layer of the Yanchang Formation

(Table 4). Trace element values were normalized by primitive mantle values (Taylor and McLennan 1985; Sun and McDonough 1989) to plot a spider diagram (Fig. 6) with high peaks for Rb, Pb, Zr, Ba, Zn, and U content. All samples of the tuffaceous layer, including sandstone and mudstone, show similar geochemical behavior for uranium enrichment, except for samples YCF-09 (tuffaceous sandstone) and YCF-10 (sandstone).

U values were plotted against Ta, Zr, Ba, Lu, Th, Dy, Pb, and Yb. The plots show a positive correlation with Ta, Th, Pb, Lu, Dy, and Yb in tuffaceous samples and weak correlation with Ba and Zr (Fig. 7).

#### 5 Formation and source of the tuffaceous anomaly of the Yanchang Formation

To determine the formation mechanism of the tuffaceous layer of the Yanchang Formation, its silica ( $\text{SiO}_2$ ) content was plotted against  $\text{TiO}_2$  (Tarney 1976). As previous studies have shown, few elements in the tuffaceous material remain unaltered by weathering or other diagenetic processes;  $\text{TiO}_2$ , for example, is very resistant (Huff et al. 1997). All but one sample plotted as sedimentary rocks; the exception was of igneous origin (Fig. 8). This suggests the tuffaceous layer resulted from deposition of volcanic ash and other sedimentary material that travelled a long distance from the source area. Through transportation and diagenetic effects, volcanic ash was altered to be sedimentary material.

Explosive volcanoes produce a large amount of volcanic ash and very fine-grained material with a tendency to travel a long distance before deposition. Such fine material and volcanic ash deposited in sedimentary basins change to clay particles (Huff et al. 2010). If the volcanic ash or fine particles remain unaltered, they can help determine the

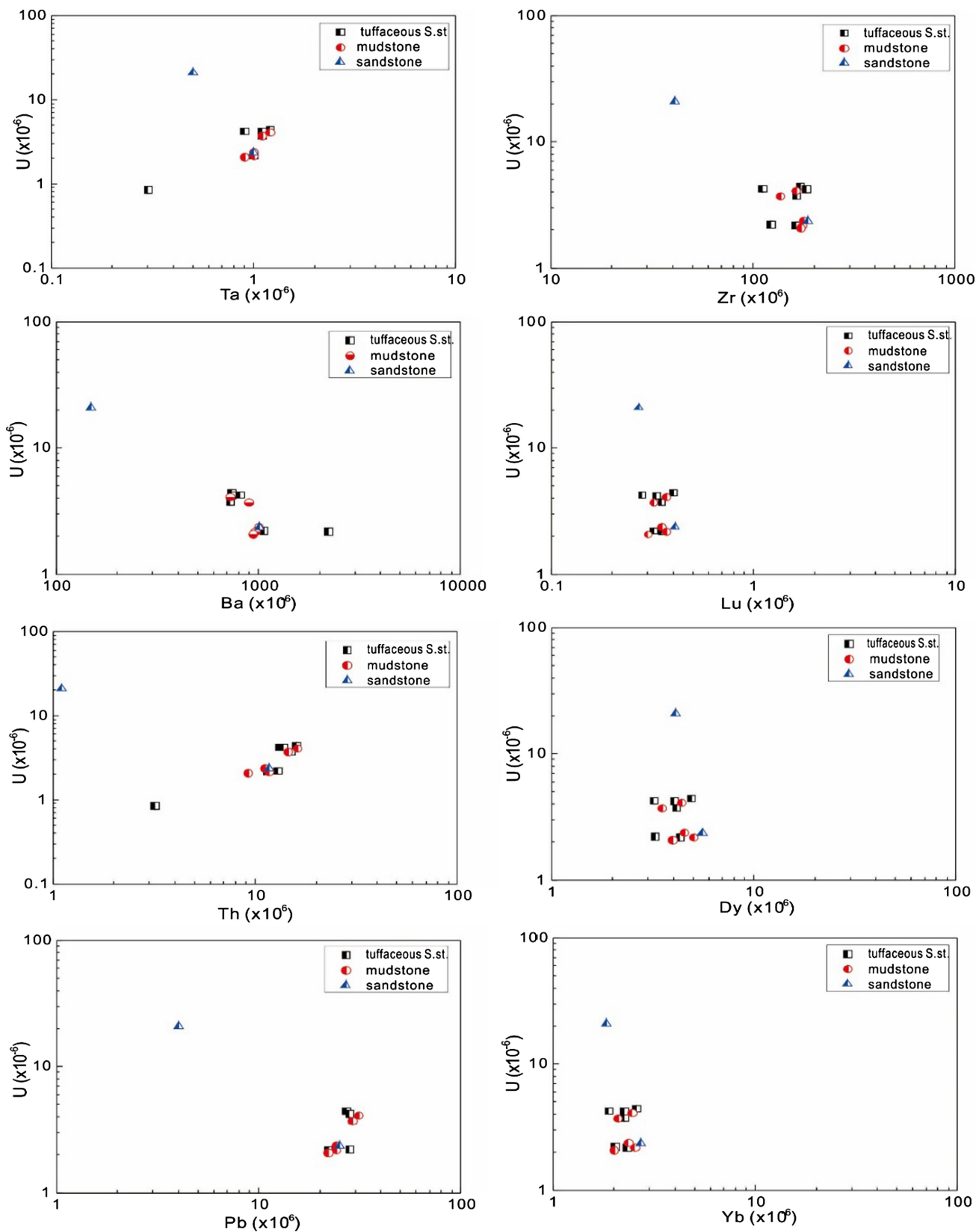


**Fig. 7** Correlation of uranium content of tuff layer with other trace elements and rare earth elements

composition and mineralogy of source magma (Gorton and Schandl 2000; Sharma et al. 2005).

### 5.1 Tectonic setting of the host volcanoes

To determine the tectonic setting of volcanoes that provided the material for the tuffaceous layer in the Upper Triassic Yanchang Formation, volcanic ash data were plotted on discrimination diagrams of Th/Yb versus Ta/Yb (Fig. 9A) (Schandl and Gorton 2002) and Th/Hf versus Ta/Hf (Fig. 9B) (Pearce et al. 1984). In both plots, all samples fell in the area of an active continental margin, the presumed tectonic setting of source volcanoes.

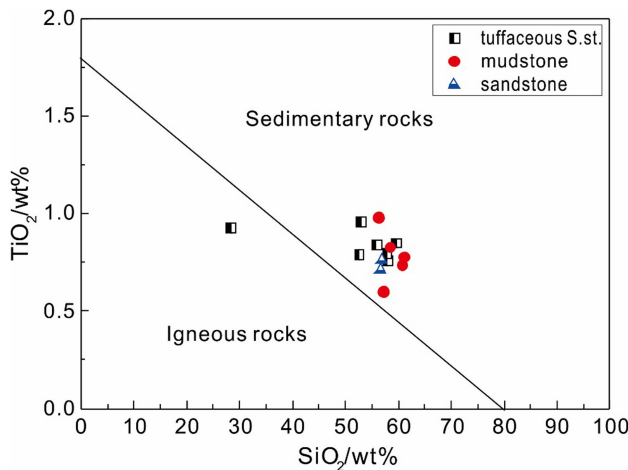


**Fig. 8**  $\text{SiO}_2$  versus  $\text{TiO}_2$  for tuffaceous material of the Yanchang Formation, Ordos Basin (Lai et al. 2010)

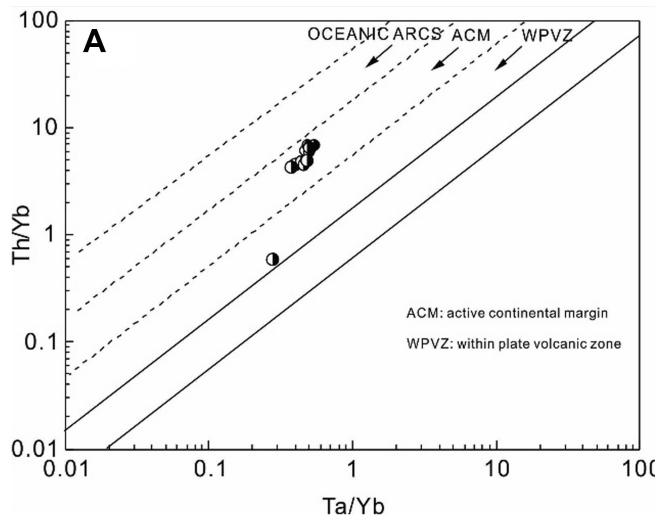


**Fig. 9** Tectonic discrimination diagram for source volcanoes by plotting Th/Yb versus Ta/Yb (A) (Schandl and Gorton 2002) and Th/Hf versus Ta/Hf (B) (Pearce et al. 1984)

### 5.2 Type and composition of source rock

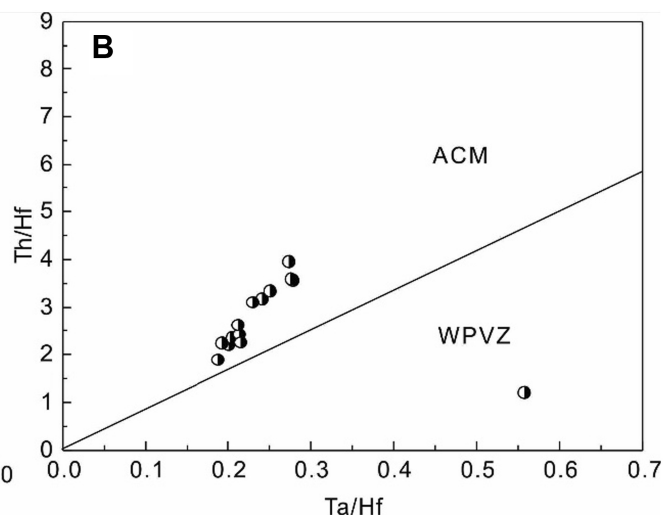
To find the rock type of source volcanoes, Rb versus  $\text{Y} + \text{Nb}$  (Fig. 10A) and Nb versus  $\text{Y}$  (Fig. 10B) were plotted (Pearce 1982). The plots show that the tuffaceous sediments of Yanchang Formation belong to “volcanic arc granite.”

To find the composition of the source arc granite,  $\text{TiO}_2$  versus Zr was plotted (Fig. 11A); most samples fell in the area of calc-alkaline arc magma. REE distribution patterns (Fig. 4) with negative Eu anomalies, enrichment of LREEs, and depletion of HREEs, support the results of the compositional discrimination diagrams. Consequently, we posit that the source magma of the tuffaceous sediments is calc-alkaline arc related. To determine whether this arc-related magma belongs to an island arc or continental arc, Th/Yb versus Nb/Yb was plotted (Fig. 11B); all the tuffaceous samples fell within the continental arc field. Therefore, we conclude that source rocks of the tuffaceous layer belong to calc-alkaline, continental arc-related volcanoes.

### 6 Enrichment of uranium in the tuffaceous layer

The tuffaceous layer of the Yanchang Formation has high gamma ray values due to high content of uranium. Although the uranium content of the tuffaceous layer was previously determined to be not more than  $3 \times 10^{-6}$  (Lai et al. 2010), our tuffaceous layer rock samples returned uranium content up to  $4.44 \times 10^{-6}$ , with one sandstone sample at  $20.9 \times 10^{-6}$ .

The tuffaceous layer lies in the Yanchang Formation of Upper Triassic strata that underly Jurassic strata. Both the Yannan and Zhilou Formations have high contents of



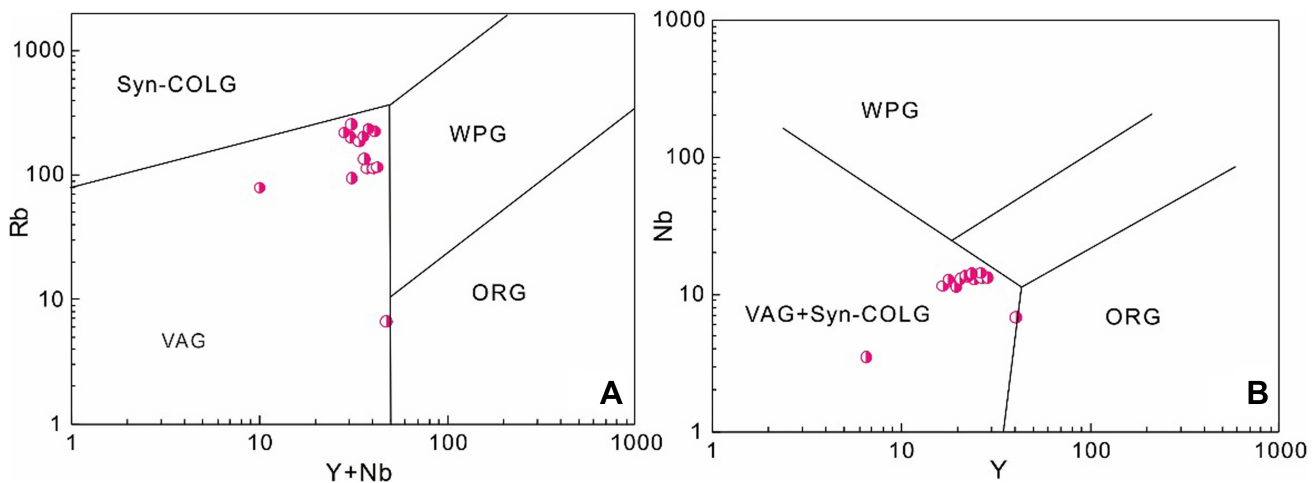


**Fig. 10** Tectonic discrimination diagrams for the source volcanoes of the tuffaceous layer after (Pearce 1982). VAG volcanic arc granite, Syn-COLG syn-continental granites, WPG within plate granite, ORG oceanic ridge granite

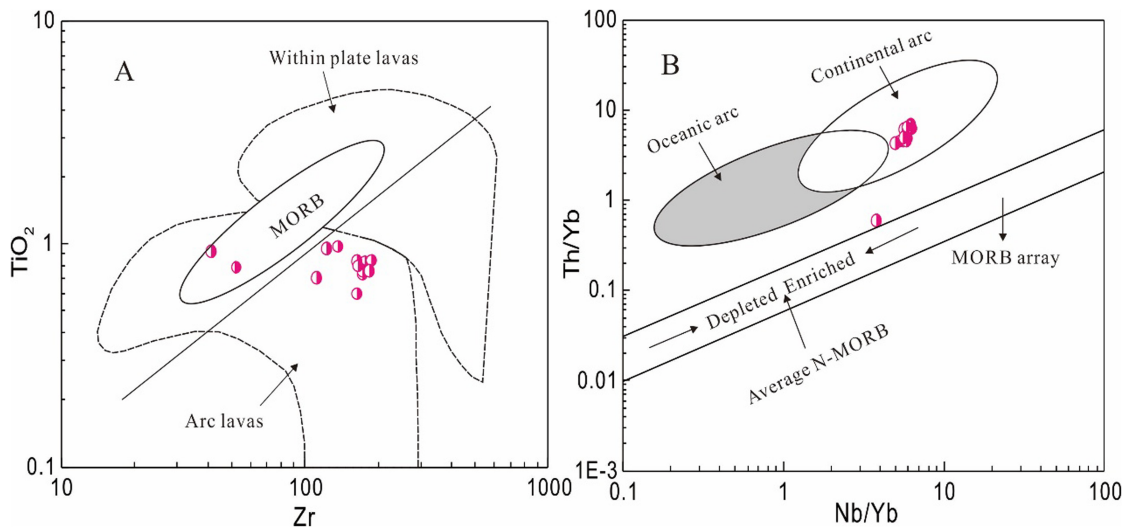


**Fig. 11** Discrimination diagram of source arc granite composition **A** after Pearce and Peate (1995), **B** after Gao et al. (1998)

uranium, petroleum, coal, and natural gas, and play an important role in uranium enrichment of the tuffaceous layer. The Yanchang Formation itself is a good reservoir of petroleum. The Yanchang was deposited in the Upper Triassic as eroded sediments of the Yinshan and the Qinling Mountains were deposited in fluvial-deltaic and lacustrine environments (Li et al. 2009; Zou et al. 2012). The intraplate Ordos Basin then developed and various evolutionary stages changed the depositional environment. In the Late Triassic, erosion of Liupan Mountain caused isostatic rebound resulting in an unconformity between the Triassic and Jurassic strata (Liu 1998). Moreover, strong tectonic activity occurred during the Late Triassic to Early Cretaceous, including the collision of the China and Qiangtang Blocks with the Eurasian Plate. Such tectonic activity developed a large number of fissures and gaps in

this area through which uranium-enriched fluid moved downward from the Jurassic strata to the Yanchang Formation. Due to pressure relief, natural gases such as CH<sub>4</sub>, H<sub>2</sub>S, CO, CO<sub>2</sub> and H<sub>2</sub>, started to move up. The tuffaceous layer acts as a barrier for downward flowing fluids and upward moving gases. Consequently, the speed of rapidly penetrating uranium-bearing fluids decreased, allowing the fluids to interact with the gases. Penetrating fluids were oxidizing, having U<sup>6+</sup>, a soluble form of uranium. However, after interaction with reducing natural gases, hexavalent uranium (U<sup>6+</sup>) started to reduce into tetravalent uranium (U<sup>4+</sup>). As tetravalent uranium is insoluble in water and other fluids, uranium precipitated in the tuffaceous layer. A schematic for uranium enrichment in the tuffaceous layer of the Yanchang Formation (Fig. 12) shows uranium enrichment in the tuffaceous layer

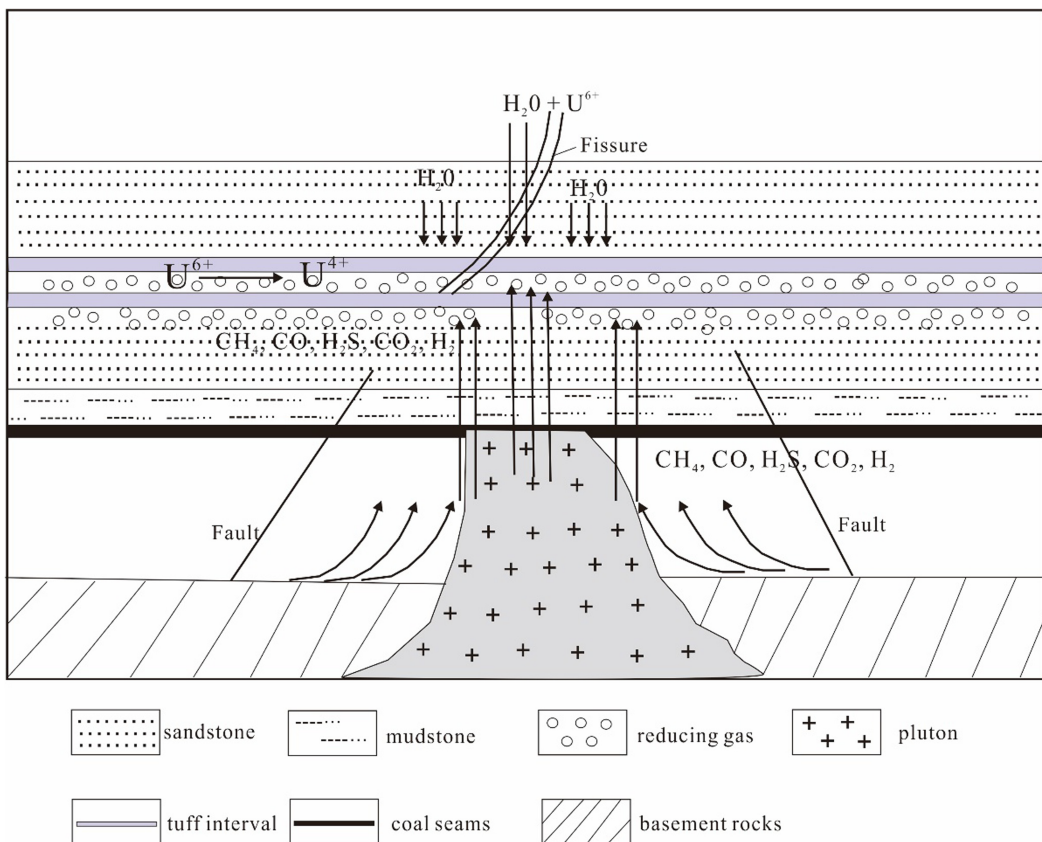


**Fig. 12** Model for mechanism of uranium enrichment in the tuffaceous layer of the Triassic Yanchang Formation, modified after Lai et al. (2010)

enhanced by tectonic activity and by oxidation–reduction processes.

## 7 Conclusions

- (1) The high gamma-ray tuffaceous layer, hosted by the Yanchang Formation of the Ordos Basin is matrix-supported with sub-rounded to sub-angular lithic fragments. These lithic fragments likely derived from pre-existing rocks and incorporated into the tuff during volcanic eruption.
- (2) The tuffaceous sediments originated as an intermediate magma. Specifically, tectonic and compositional discrimination diagrams show the tuffaceous layer belongs to calc-alkaline continental arc-related magma.
- (3) After deposition of the tuffaceous layer, uranium enrichment resulted from tectonic activity. A large number of fissures and gaps developed, allowing uranium-enriched fluids to migrate downward from Jurassic strata while natural gases rose due to pressure relief, developing an oxidation–reduction boundary to enhance uranium enrichment.

**Acknowledgements** This work was supported by National Program on Key Basic Research Project (973 Program) (2015CB453002), DREAM Project of MOST China (2016YFC0600404), and CAS-TWAS President Fellowship 2012.

## References

- Cai CF, Dong HL, Li HT, Xiao XJ, Ou GX, Zhang CM (2007) Mineralogical and geochemical evidence for coupled bacterial uranium mineralization and hydrocarbon oxidation in the Shashagetai deposit, NW China. *Chem Geol* 236:167–179
- Coveney RM Jr, Glascock MD (1989) A review of metal-rich Pennsylvanian black shales, central USA, with an inferred role for basinal brines. *Appl Geochem* 4:347–367
- Coveney RM Jr, Martin SP (1983) Molybdenum and other heavy metals of the Mecca Quarry and Logan Quarry Shales. *Econ Geol* 78:132–149
- Coveney RM Jr, Leventhal JS, Glascock MD, Hatch JR (1987) Origins of metals and organic matter in the Mecca Quarry Shale member and stratigraphically equivalent beds across the Midwest. *Econ Geol* 82:915–933
- Disnar JR, Sureau JF (1989) Organic matter in ore genesis: progress and perspectives. *Org Geochem* 16:577–599
- Doveton JH, Merriam DF (2004) Borehole petrophysical chemostratigraphy of Pennsylvanian black shales in the Kansas subsurface. *Chem Geol* 206:249–258
- Gao S, Luo TC, Zhang BR, Zhang HF, Han YW, Zhao ZD, He YK (1998) Chemical composition of the continental crust as revealed

- by studies in east China. *Geochim Cosmochim Acta* 62:1959–1975
- Gorton MP, Schandl ES (2000) From continent to island arcs: a geochemical index of tectonic setting for arc related and within plate felsic to intermediate volcanic rocks. *Can Mineral* 38:1065–1073
- Hu L (2010) The geological–geochemical characteristics and genesis of the main epigenetic alteration in the Dongsheng uranium area of the Ordos Basin. Master's dissertation, Northwest University, China
- Huff WD, Bergstrom SM, Kolata DR, Sun HP (1997) The lowest Silurian Osmundsb erg K-bentonite part II mineralogy, geochemistry, chemo stratigraphy and tectonomagmatic significance. *Geol Mag* 135(1):15–26
- Huff WD, Bergstrom SM, Kolata DR (2010) Ordovician explosive volcanism. In: Finny SC, Berry WBN (eds) The Ordovician Earth system, Geological Society of America Special Paper, vol 466, pp 13–18
- Lai XD, Yang XY, Gao P, Wu BL, Liu CY, Sun WD (2010) Geochemical study on uranium rich tuffs in Yanchang groups in the southern Ordos Basin: implication to their forming mechanism. *Chin J Geol* 45(3):757–776 (in Chinese with English abstract)
- Leventhal JS (1993) Unanswered questions about organic matter and ore deposits and new directions for research. *Geological Society of America Abstracts with Programs* 25:A-29
- Li RX, Li YZ (2008) Tectonic evolution of the western margin of the Ordos Basin (Central China). *Russ Geol Geophys* 49:23–27
- Li RX, Li YZ (2011) The geologic features of mineralization at the Dongsheng uranium deposit in the northern Ordos Basin (Central China). *Russ Geol Geophys* 52:593–602
- Li S, Yang S, Jevzy Kiewicz T (1995) Upper Triassic–Jurassic foreland sequences of the Ordos Basin in China. In: Stratigraphic evolution of foreland basins, SEPM Special Publication, vol 52, pp 233–241
- Li GR, Guo QY, Shi YL (2006) Research on identifying the reservoir of high gamma in Ordos Basin. *World Well Logging Technol* 21:33–35 (in Chinese with English abstract)
- Li WH, Pang JG, Gao HX, Xiao L, Wang RG (2009) Depositional system and paleogeographic evolution of the late Triassic Yanchang stage in Ordos Basin. *J Northwest Univ* 39(3):501–506 (in Chinese with English abstract)
- Liu SF (1998) The coupling mechanism of basin and orogeny in the western Ordos Basin and adjacent regions of China. *J Asian Earth Sci* 16:369–383
- Liu J-S (1992) Analysis of the geological characteristics of the Carboniferous–siliceous–argillaceous uranium deposits in South China. *Collect pap geopol prospect* 7:103–110 (in Chinese)
- Liu HQ, Li XB, Liao JB, Liu XY (2013) Genesis of the high magma sandstone of the Yanchang Formation in the Ordos Basin, China. *Pet Sci* 10:50–54 (in Chinese with English abstract)
- Pearce JA (1982) Trace element characteristics of lavas from destructive plate boundaries. In: Thorpe RS (ed) Andesite. Wiley, Chichester, pp 525–548
- Pearce JA, Peate DW (1995) Tectonic implication of the composition of volcanic arc magmas. *Annu Rev Earth Planet Sci* 23:251–285
- Pearce JA, Harris N, Tindle A (1984) Trace elements discrimination diagrams for the tectonic interpretation of granitic rocks. *J Petrol* 15:956–983
- Qiu XW, Liu CY, Mao GZ, Wang JQ (2009) Distribution characteristics and geological significances of tuff interlayers in Yanchang Formation of Ordos Basin. *Acta Sedimentol Sin* 27:1138–1146 (in Chinese with English abstract)
- Qiu XW, Liu CY, Mao GZ, Deng Y, Wang FF, Wang JQ (2014) Late Triassic tuff intervals in the Ordos Basin, Central China: their depositional, petrographic, geochemical characteristics and regional implications. *J Asian Earth Sci* 80:148–160
- Schandl ES, Gorton MP (2002) Application of high field strength elements to discriminate tectonic settings in VMS environment. *Econ Geol* 97:629–642
- Sharma S, Dix GR, Villeneuve M (2005) Petrology and potential tectonic significance of a K-bentonite in a Taconian shale basin (eastern Ontario, Canada), northern Appalachian. *Geol Mag* 142(2):145–158
- Spirakis CS (1996) The roles of organic matter in the formation of uranium deposits in sedimentary rocks. *Ore Geol Rev* 11:53–69
- Sun P, Zhang XL, Guo L (2010) Genesis of the sandstone with higher radioactivity and the quantitative evolution of its reservoir property: taking Chang 6 oil bearing strata in Zhidan oilfield, Ordos Basin as an example. *J Xi'an Shiyou Univ (Nat Sci Edit)* 25:18–21 (in Chinese with English abstract)
- Sun SS, McDonough WF (1989) Chemical and isotopic systematics of oceanic basalts, implication for mantle composition and processes. In: Saunders AD, Norry MJ (eds) Magmatism in the Ocean Basins. Geological Society of London, pp 313–345
- Swanson VE (1956) Uranium in marine black shales of the United States. US Geological Survey Professional Paper, pp 451–456
- Tarney J (1976) Geochemistry of Archean high grade gneisses, with implications as to the origin and evolution of the Precambrian crust. In: Windley BF (ed) The early history of the Earth. Wiley, London, pp 405–417
- Taylor SR, McLennan SM (1985) The continental crust. Its composition and evolution. Blackwell, Oxford, pp 9–56
- Wang ZG, Yu XY, Zhao ZH (1989) Rare-Earth element geochemistry. Science Press, Beijing, pp 1–535 (in Chinese with English abstract)
- Wang ZT, Zhou HR, Wang XL, Jing XC (2015) Characteristics of the crystalline basement beneath the Ordos Basin: constraint from aeromagnetic data. *Geosci Front* 6:465–475 (in Chinese with English abstract)
- Yang JJ (2002) Tectonic evolution and the distribution of petroleum in the Ordos Basin, China. Petroleum Industry Press, Beijing, p 15 (in Chinese with English abstract)
- Yang XY, Ling MX, Sun WD, Lai XD, Liu CY, Miao JY, Sun W (2009) The genesis of sandstone type uranium deposits in the Ordos Basin, NW China: constraints provided by fluid inclusions and stable isotopes. *Int Geol Rev* 51:422–455
- Yuan YS, Hu SB, Wang HJ, Sun FJ (2007) Meso-Cenozoic tectonothermal evolution of Ordos Basin, central China: insight from newly acquired vitrinite reflectance data and a revision of existing paleothermal indicator data. *J Geodyn* 44:33–46
- Zhang XQ, Liao CZ, Shi W, Hu B (2006) Neotectonic evolution of the peripheral zones of the Ordos Basin and geodynamic setting. *Geol J China Univ* 12:285–297 (in Chinese with English abstract)
- Zhang XL, Feng Q, Sun P, Li W (2010) Characteristics of high-gamma-ray sandstone reservoirs for Yanchang Formation in Ordos Basin. *Chin J Geophys* 53:154–163 (in Chinese with English abstract)
- Zhao HG (2005) The relationship between tectonic-thermal evolution and sandstone type uranium ore formation in Ordos Basin. *Uranium Geol* 21:275–282 (in Chinese with English abstract)
- Zhao JL, Tan CQ, Liu CY (2006) Abnormal features of obvious natural gamma in Ordos Basin. *J Earth Sci Environ* 28:82–86 (in Chinese with English abstract)
- Zou CN, Wang L, Li Y, Tao SZ, Hou LH (2012) Deep-lacustrine transformation of sandy debrites into turbidites. Upper Triassic, Central China. *Sediment Geol* 265–266:143–155